TECHNICAL REPORT

SPACE TELESCOPE SCIENCE INSTITUTE
Operated for NASA by AURA

Title: Simulations of Target Acquisition with MIRI Four-Quadrant Phase Mask Coronagraph (I).	Doc #: JWST-STScI-003063, SM-12 Date: September 26, 2012 Rev: -
Authors: Rémi Soummer, Dean Hines, Marshall Perrin Phone: 410 - 338 - 4737	Release Date: January 7, 2013

1 Abstract

This report studies coronagraphic target acquisition (TA) with MIRI four quadrant phase mask coronagraphs (FQPMs). We present a new set of simulations showing that the FQPM impacts the centroid measurements during TA for target positions within about 1 arcsec from the center. The effect on the centroid is small but non-negligible compared to the alignment requirements (10 mas from the center for the target, 5 mas between reference and target). These simulations results suggest that i) Scenarios using iterative TA at the center of the mask are problematic because of centroid errors ii) Scenarios using an intermediate TA positions require TA further away from the center of the mask where slew accuracy is no longer optimal iii) Twin-TA scenarios using symmetric positions can be used to mitigate the error introduced by the FQPM but concerns remain because the TA error budget does not meet the 5mas requirement between target and reference.

2 Introduction

The MIRI instrument includes four coronagraphs, three FQPM masks optimized to work in narrow bands (10.65,14.40 and 15.50 μm), and a classical Lyot coronagraph to work in a broad band around 23 μm. FQPM coronagraphs have the advantage to enable the detection of a companion very close to their parent star (small inner working angle), which in turn make them very sensitive to alignment.

Target acquisition (TA) is required for MIRI coronagraphs, and consists of acquiring images at some offset position from the center of the mask. Centroid measurements are then used to determine the appropriate slew to place the target precisely at the center of the mask. TA with MIRI FQPMs is performed using a neutral density (ND) filter (or possibly other broad band filters) instead of their dedicated science narrow-band filter. The purpose of the ND filter is to minimize the effect of the coronagraph on the shape of the PSF and also to avoid saturation.

In full coronagraphic mode (with matched Lyot stop and narrow-band science filter, the coronagraphic point spread function (PSF) does not resemble a standard imaging PSF: it

does not have a well-defined central core and it is mostly formed of speckles. Therefore this type of PSFs would not be suitable for TA. Moreover, the coronagraphic PSF shape changes dramatically with the position of the target from the center of the coronagraph outwards as the coronagraphic suppression decreases. Outside of the IWA the effect of the coronagraph becomes progressively negligible.

An ND filter was implemented to minimize this effect during TA. The ND filter has a very broad band, which renders the coronagraph almost inefficient, and therefore makes the coronagraphic PSF almost identical to a normal PSF with well-defined core, appropriate for centroid measurements.

Figure 1 shows simulated coronagraphic PSFs with increasing distance from the center of the coronagraph using the ND filter with the cold stop. Note that even with the ND filter, there are some minor changes in the shape of the PSF. The purpose of this report is to quantify the impact of this effect on the floating-window centroid algorithm that is used on board JWST during TA.

Because we are interested in very small effects when the target is very close to the center of the FQPM, we also developed a new propagation algorithm to take into account the actual shape of the FQPM.

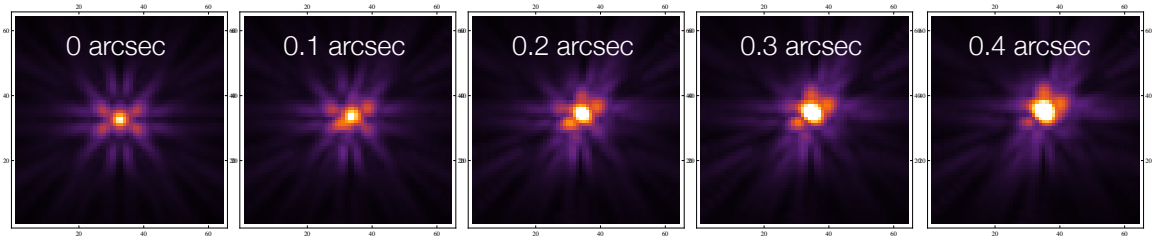

Figure 1 Coronagraphic PSF with the 10.65 µm FQPM with ND filter. The broad band minimizes the effect of the coronagraph on the PSF to enable TA. However, for positions offsets of the order of the FWHM of the PSF (~300 mas) the shape is sufficiently modified by the FQPM to impact the centroid measurement. For larger distances (~1 arcsec) this effect vanishes.

3 Target Acquisition with MIRI FQPM coronagraphs

3.1 TA Requirements

The alignment accuracy requirements for the FQPM are 10 mas for the science target, and 5 mas between the reference target and the science target.

These requirements are challenging for a number of reasons:

- 5mas corresponds to about 1/20th of a pixel (110 mas/pixel)
- The slew accuracy depends on the slew distance, with a requirement of 5mas (one-σ per axis) for slews smaller than 0.5 arcsec, and 10mas (one-σ per axis) for slews of about 1 arcsec. An initial slew from a large distance (10 arcsec) is affected by a 20mas accuracy (one-σ per axis)
- Jitter is also of the same order of magnitude with a requirement value of 7mas (one-σ per axis) with the goal of reaching 7mas radial.

3.2 TA Scenarios

There are currently two scenarios considered for TA.

- Scenario 1 (Cavarroc et al. 200X)

In this scenario, target acquisition starts at 10 arcsec from the center of the FQPM. A first slew brings the star within one pixel of the center, with an accuracy of 20mas (one-σ per axis). Several iterations include centroid measurement followed by small slew (5mas one-σ per axis) until the requirement is reached.

- Scenario 2 (Gordon & Meixner 2008 TR)

  In this scenario, TA begins at 10 arcsec from the center of the FQPM. A first slew brings the star to an intermediate position within 0.5 arcsec from the center, with an accuracy of 20mas (one-σ per axis). A single small slew (5mas one-σ per axis) brings the star to the center of the mask.

The motivations for considering scenario #2 included avoiding overheads associated with iterations, and that the actual shape of the coronagraph might impact the PSF shape (and therefore the centroid position) when the star is almost centered on the coronagraph.

Other possible variations on these scenarios include multiple acquisitions on both sides of the coronagraph center to improve the accuracy.

4 Simulations

4.1 Simulation tools

We used two independent codes: the JWCorPSF python code, and a Mathematica code.

The general simulation methods for the simulation of FQPM images are described in Soummer et al. 2010 TR, and the standard method uses Fast Fourier Transforms (FFTs). We extended the semi-analytical approach developed by Soummer et al. 2007 for Lyot coronagraphs to the case of FQPM. This simulation method enables very-high sampling of a central part of the FQPM in order to take into account the shape errors at the vertex of the phase mask. We used a micrograph from Boccaletti et al. to produce a high-resolution model of the FQPM within one resolution element (lambda/D) at the center of the mask (Figure 2) The resolution in this simulation would require 3million by 3million FFTs using the standard method. The simulation method will be described in more details in a future report.

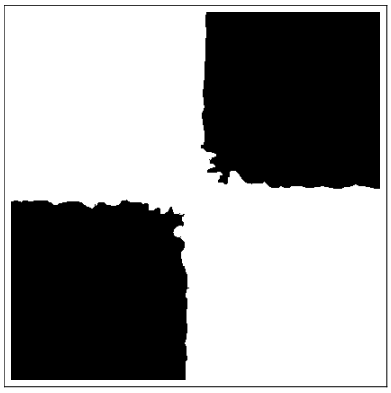

Figure 2 model of the FQPM used for the high-resolution propagation. The FQPM is assumed perfect outside of this central region up to one resolution element (lambda/D). This model is based on a micrographic image from Boccaletti et al. and rescaled to the proper plate scale. The image above corresponds to a quarter of a resolution element at 10.65 µms. We assume perfect pi-phase shift and constant index of refraction with wavelength.

For the centroid measurements, we implemented the floating-window centroid algorithm as described in Valenti et al. 2011 TR. We verified our implementation of the floating

centroid with another implementation of the code by Mike Regan (TR) and obtained measurement differences of the order of 1/1000th of a pixel between both codes. We also used a Monte-Carlo simulation to evaluate the standard deviation of the error caused by the algorithm (Figure 3), and find σx=σy=0.003 pixel, which is completely negligible compared to the effects described in this document.

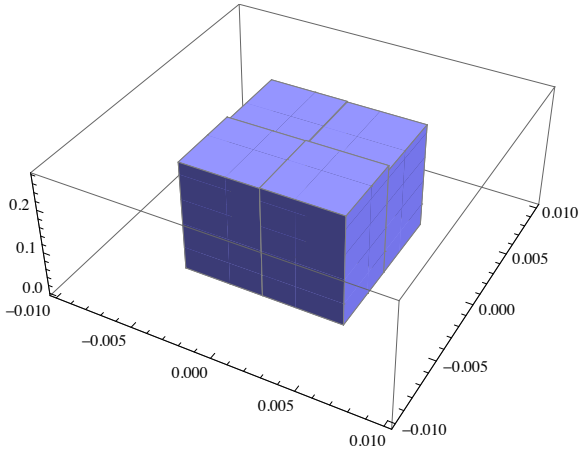

Figure 3 Histogram of the x and y accuracy of the floating-window centroid algorithm, obtained from 10,000 measurements of the PSF centroid at random location within a 2x2 pixel region, and using a 7x7 pixel boxsize. The standard deviation is σx=σy=0.003 pixel, completely negligible compared to other effects presented in this study.

4.2 Assumptions for the simulation

The assumptions used in these simulations are:

- 30 wavelengths equally spaced from 3 μm to 25 μm
- Germanium and ND transmissions, and detector quantum efficiency as a function of wavelength
- Solar-type star, assuming a black body profile.
- Perfect shape FQPM, or plausible shape using a micrograph within one resolution element (~300mas at 10.65 μm).
- Perfect pi-phase shift at the design wavelength (10.65 μm)
- Constant index of refraction for the germanium (we do not have the dispersion relationship for the germanium)
- All simulations are done for one FQPM (10.65 μm), but are scalable.
- Coronagraphic PSFs are calculated with a 4x oversampling and re-binned to the MIRI pixel size.
- Wavefront errors (WFE) maps corresponds to error budget revT, which are publicly available as part of the JWPSF distribution. WFE maps represent independent realizations of the mirror, and do not account for temporal correlation.
- Perfect detector, no photon noise, no cosmic rays or other artifact
- Floating centroid algorithm with a 7x7 pixel box
- Field of view limit of 23 arcsec

- Jitter is simulated using 25 positions on a regular grid ranging from -20 mas to +20 mas in x and y coordinates. The final PSF is obtained using a weighted average with a Gaussian distribution of radial standard deviation 10 mas. This assumes that the jitter timescale is much smaller than the exposure time.

4.3 Simulation results

We generate simulated TA coronagraphic PSFs through the 10.65μm FQPM with the ND filter. The PSFs are calculated along the 45-degree direction relative to the edges of the phase mask. We apply the floating centroid algorithm to measure the PSF position and compare measured position with the true position where the target is located.

Figure 4 shows the measured position using the centroid algorithm as a function of the true position of the target, and Figure 5 the difference between the measured position and the true position. In this simulation wavefront error maps have been corrected from tilt so that the true position of the target with respect to the mask center is well known. The tilts were removed according to the floating centroid measurement for the un-occulted PSF to insure consistency in the simulation.

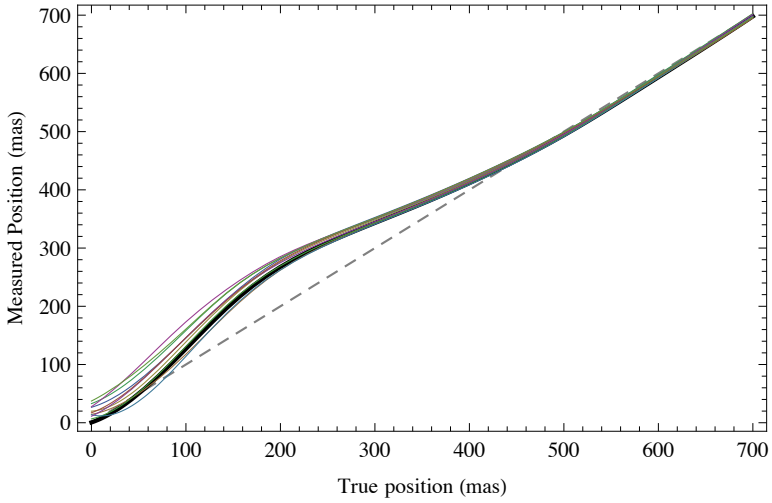

Figure 4: Measured position using the floating centroid algorithm as a function of the true position of the star from the center of the FQPM along the 45-degree axis. The black line corresponds to a hypothetical case without wavefront error (perfect telescope). The colored lines show the error and dispersion for 10 independent realization wavefront error realizations (Rev T error budget). This simulation is done using standard FFT propagation, and without jitter.

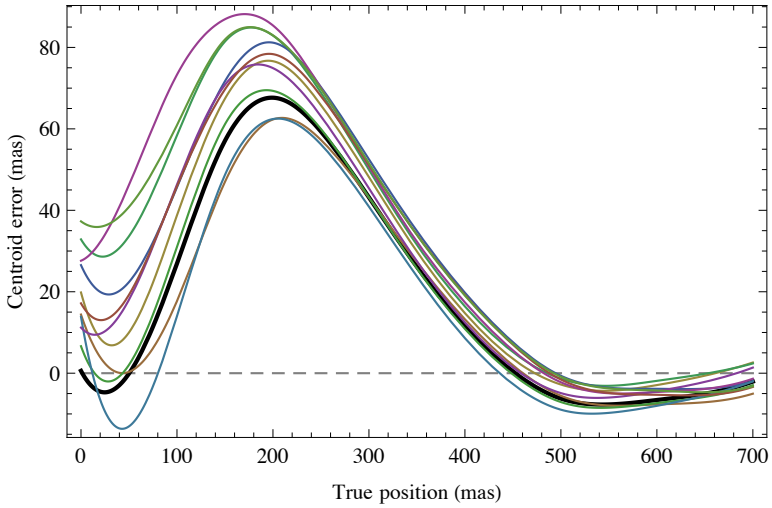

Figure 5 Difference between the measured position and true position corresponding the same simulation shown in Figure 4. The separation needs to be at least 0.6 or 0.7 arcsec to be of the order of 10mas. At a wavelength of 10.65 µm the FWHM of the PSF is ~300 mas. The impact of the FQPM on the centroid is significant for TA, up to a distance about twice the FWHM of the PSF. Note that this effect scales with wavelength so that for the 15.5 µm FQPM the minimum separation for minimum impact on TA should be of the order of 1 arcsec. The black line corresponds to a hypothetical case without wavefront error (perfect telescope). The colored lines show the error and dispersion for 10 independent realization wavefront error realizations (Rev T error budget). This simulation is done using standard FFT propagation, and without jitter.

The simulations shown in Figure 4 and Figure 5 are based on FFT propagations and do not include Jitter. In the following we perform a number of test to check that the general effect is truly due to the FQPM and not to the simulation code assumptions or methods.

In Figure 6 and Figure 7 we compare the centroid position between the FFT Propagation method and the multi-scale propagation, in two cases: a perfect FQPM shape or a more realistic FQPM shape based on a micrographic image.

In the case of a perfect-shape FQPM the differences between the FFT propagation method and the high-resolution propagation is very small.

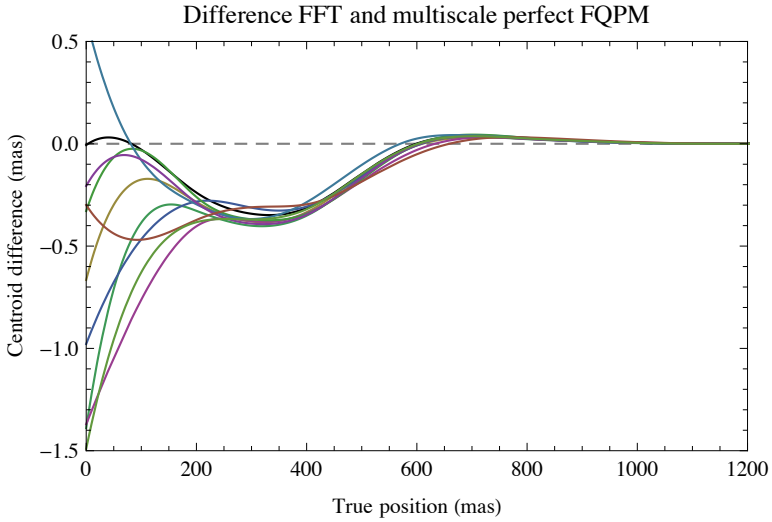

Figure 6 Difference in the centroid measurements between the standard FFT propagation and the multi-scale propagation code assuming a perfect FQPM shape. The differences are due to the difference in sampling at the center of the FQPM and are negligible for TA.

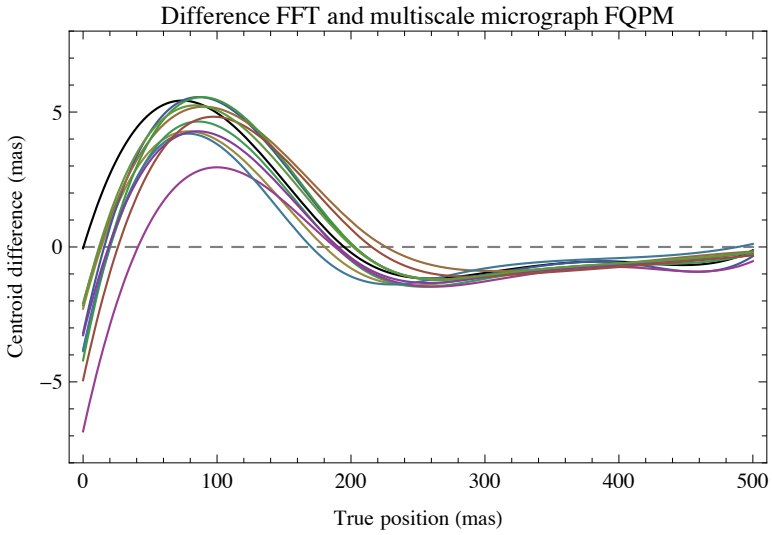

Figure 7 Same as previous figure but with a high-resolution model of the FQPM based on a micrographic image and used within one resolution element (lambda/D) at the center. The model for the FQPM is based on a micrograph image (Figure 2).

In Figure 8 we study the impact of jitter on the measured centroid. Because this simulation is extremely intensive computationally (25 positions and 30 wavelengths) and because the effect of the high-resolution propagation is negligible we use the standard FFT propagation method. In the presence of WFE the coronagraphic suppression is reduced and speckles dominate the PSF. Jitter has a very small impact on the centroid measurement.

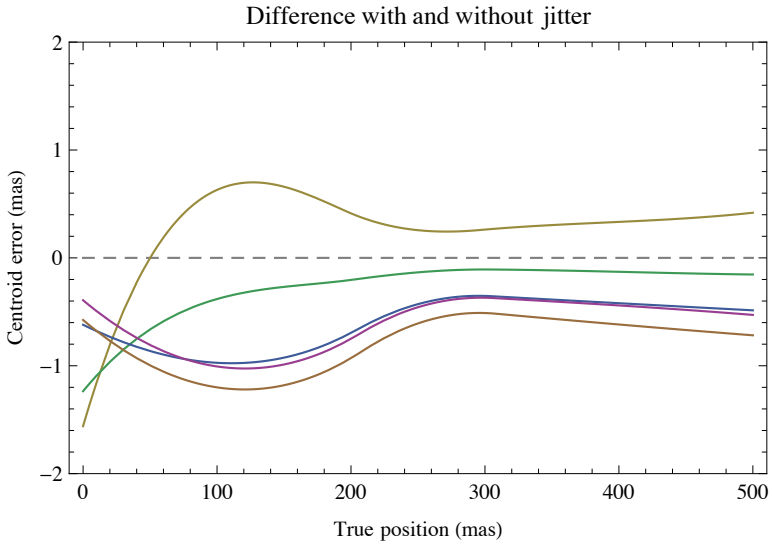

Figure 8 Difference in the centroid measurements between the simulation without jitter and with jitter. Because the simulation is extremely computationally intensive the plot only shows the case of few realizations of the wavefront error. The impact of the jitter is much smaller than the effect of the FQPM, and therefore is not a concern during TA.

5 Mitigation for target acquisition

5.1 Calibration during commissioning

One possible solution would be to try to calibrate the effect of the FQPM along the 45-degree direction during commissioning, and to compensate for the centroid position error during TA. Because of the limited accuracy of small slews, the true position could only be known using other stars in the MIRI field. Figure 9 shows the residual centroid error assuming perfect calibration, and no WFE. Similar results are obtained with any of the WFE curves. Because the wavefront will have some degree of temporal correlation, this is a pessimistic scenario in terms of the dispersion between WFEs. Even with a hypothetical perfect calibration, the residual error after calibration is of the order of 10mas at 0.7 arcsec. Although it would certainly be very interesting to acquire this type of data during commissioning to verify these centroid errors, calibration seems unlikely to be usable for TA.

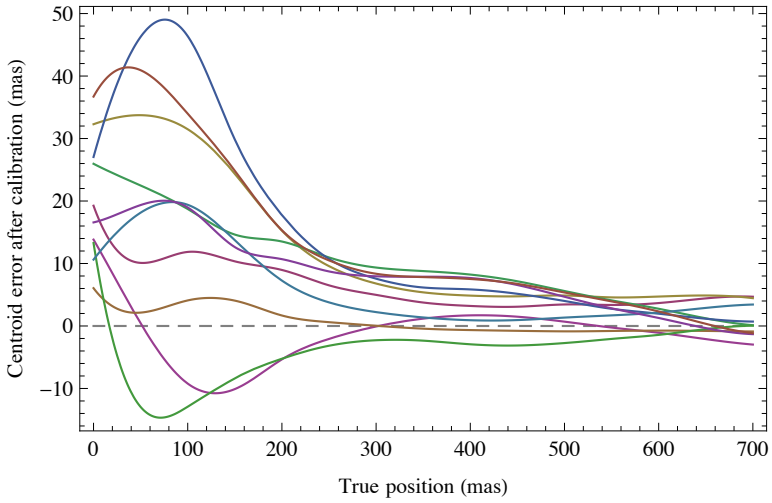

Figure 9 residual errors between the centroid measurement and the true position assuming a calibration of the error from Figure 5. The reference used for calibration is the curve without wavefront error for this example. Each color represents the residual error for an independent realization of the mirror according to the rev T error budget. Depending on the stability of the WFE with time, the calibration should be significantly better. For the 10.65µm FQPM, a calibration of the error could provide a residual error of the order of 10mas. The calibration would require a raster of star position with very fine steps using other stars in the MIRI field of view to measure precisely the true position.

5.2 Optimal TA distance

These simulations suggest that TA at intermediate positions should be placed at slightly larger distance to avoid centroid errors caused by the FQPM. The optimal distance based on these simulations is between 0.7 and 1 arcsec from the star. These numbers correspond to the 10.65 µm FQPM and need to be rescaled with wavelength for the other masks: the minimum TA distance is ~1.5 times larger for the 15.50µm FQPM.

Because the pointing accuracy requirements are degraded for slews larger than 0.5 arcsec, the combination of pointing slews accuracy and centroid errors make TA challenging. It

will be critical to know more precisely how the pointing accuracy degrades beyond 0.5 arcsec.

5.3 Twin-TA

The centroid error is symmetric on both side of the mask. A twin-TA procedure with two symmetrical positions on both sides of the FQPM vertex would be affected by opposite centroid errors from the FQPM mask, and therefore this strategy can be used to mitigate the effect of the FQPM.

A twin-TA with two symmetric positions would include the following steps:

- step0: slew to position TA#0 sufficiently far (>2arcsec) to avoid centroid errors
- step1: Slew to position TA#1, 0.5 arcsec from center along 45-degree axis
- step2: Slew to position TA#2, 0.5 arcsec from center on the opposite side
- step3: Slew to center using the average value from TA#1 and TA#2.

Because both positions would not be perfectly symmetric, the centroid error would not cancel out perfectly. Assuming a linear error in the range of true separations 200-400mas as shown in Figure 5, the centroid error is 3.5mas for 10mas of separation. Assuming that ~1 arcsec slews have an accuracy of 10mas (one-σ per axis), that the final smaller slew has an accuracy of 5mas (one-σ per axis), and that the uncompensated residual centroid error after averaging the two positions TA#1 and TA#2 is 3.5mas, the total error would be RSS[RSS[10, 3.5, 10, 3.5]/2 ,5], corresponding to 9mas, one-σ per axis, or 13mas radial, one-σ, not including jitter. Including Jitter (7mas one-σ per axis) at both TA#1 and TA#2 positions and final position we find a total error of 12.4mas one-σ per axis (17.6 mas radial, one-σ). These numbers are also problematic considering the coronagraphic requirements.

6 Conclusion

We simulated the impact of the FQPM on centroid measurements in the range of intermediate positions from 0 to 1 arcsec during coronagraphic TA with the ND filter. In order to evaluate the effects of the mask shape very close to the vertex, we developed a new propagation method based on an analytical multi-scale formulation of the wave propagation and using an efficient matrix-based Fourier transform algorithm to propagate the high-resolution component.

We find that standard simulations involving FFTs are appropriate for the purpose of TA, since the numerical error on the centroid introduced by the low sampling of the mask with FFTs is less than 5 mas compared to the more-accurate multi-scale propagation method.

For the scenario using an intermediate TA position, the optimum distance to minimize the centroid error is at least ~0.7 arcsec for the 10.65 μm FQPM which scales to ~1 arcsec for the 15.5 μm FQPM. Unfortunately this corresponds to a region where the slew accuracy is reduced to 10mas (one-σ per axis), which raises concerns when compared to the coronagraphic requirements (10mas for science target and 5mas for reference /target distance).

Based on these simulations using independent realizations of the WFE (“rev T” error budget), there are also concerns with the scenario involving iterations at the center of the mask because the centroid error from the FQPM can be up to 40mas. New simulations

with updated WFE maps including temporal correlation based on thermal modeling would be required to fully evaluate the feasibility of this iterative scenario.

Because the centroid error is symmetric on both sides of the mask, a possible variant of these scenarios is to use one or more pairs of TA positions ("Twin-TA") so that the error on centroid measurements introduced by the FQPM is compensated in part.

Also, small dithers can be considered to improve performance but they would need to be implemented in the coronagraphs scripts, and would require to be able to perform small slews under fine guidance to minimize overhead.

Future simulations (see Lajoie, Soummer, & Hines 2012) will be necessary to fully investigate the limitations and implementation of the MIRI Coronagraphs TA.

7 References

Boccaletti, A., Baudoz, P., Baudrand, J., Reess, J.M., Rouan, D. 2005. Imaging exoplanets with the coronagraph of JWST/MIRI. Advances in Space Research 36, 1099-1106

Cavarroc, C., Boccaletti, A., Baudoz, P., Amiaux, J., Regan, M. 2008. Target Acquisition for MIRI Coronagraphs. PASP 120, 1016-1027.

Cox, C., Hodge, P. 2006. Point-spread function modeling for the James Webb Space Telescope. SPIE Conference Series 6265

Gordon K. Meixner, M. 2008 Mid-InfraRed Instrument (MIRI) Target Acquisition Strategies and Use Cases STScI Technical Report, JWST-STScI-001407

Lajoie, C.-P., Soummer, R., & Hines, D.C. 2012, JWST-STScI submitted

Soummer , R. , Makidon, R. 2010, Simulations of MIRI coronagraphic images, STScI technical report, JWST-STScI-001952

Soummer, R., Pueyo, L., Sivaramakrishnan, A., Vanderbei, R.J. 2007. Fast computation of Lyot-style coronagraph propagation. Optics Express 15, 15935